Activation and regulation of E. coli DNA Polymerase V studied at the single-molecule level

Caldas, Victor Emanoel Armini

5

Pol V does not compete with other TLS polymerases

Victor E.A. Caldas, Elizabeth A. Wood, Michael M. Cox, Roger Woodgate, Myron F. Goodman, Antoine M. van Oijen, Andrew Robinson.

DNA polymerase V does not compete with DNA polymerases II and IV for binding sites on DNA in UV-irradiated *Escherichia coli* cells. *Manuscript in preparation.*

Abstract

Escherichia coli contains five DNA polymerases (Pols). Pols I and III accurately replicate DNA under normal conditions, but are unable to copy damaged DNA. Pols II, IV and V are induced by DNA damage and carry out error-prone translesion DNA synthesis (TLS). Although the biochemical activities of the Pols are well known, there are many open questions surrounding the regulation and competition between the Pols in vivo. Because these proteins are expressed at extremely low levels, single-molecule fluorescence microscopy allows us to test if current models for the coordination of TLS DNA polymerases hold true in living cells. We have fused Pol V to mKate2 and the τ-subunit of the replisome to YPet, keeping both fusions controlled by their respective promoters. We investigated the influence of other TLS polymerases, as well as the DNA damage response protein RecA, on the cellular location, expression levels and access of Pol V to DNA. Our results suggest that RecA acts as a 'traffic cop' directing Pol V to lesions at sites distinct from replisomes. Pols II and IV have little effect on the number of Pol V molecules bound to replisomes or other sites on the chromosome.

5.1. Introduction

Escherichia coli has five DNA polymerases (Pols), which differ in speed, processivity, and fidelity when synthesizing DNA [1]. They can be divided into two main groups. Pols I and III are high-fidelity polymerases responsible for bulk replication of the chromosome. Pols II, IV and V are specialized translesion synthesis (TLS) polymerases expressed in response to DNA damage. TLS polymerases, as opposed to the replicative polymerases, have the capacity to incorporate nucleotides opposite damage sites on the template DNA. However, the TLS polymerases are highly error prone and thus mutagenic. While synthesizing DNA, all five Pols interact with the β-sliding clamp, a homodimeric protein that encircles the DNA and acts as a processivity factor [2]. Each β-sliding clamp contains two identical binding sites, which can be occupied by conserved penta- or hexa-peptide motifs that are found within many DNA replication and repair proteins [3]. The β-sliding clamp acts as a protein interaction hub, serving to coordinate DNA replication and repair; a mechanism conserved across bacteria [4]. The trimeric PCNA clamp performs a similar role in eukaryotes [5].

How do *E. coli* cells coordinate the activities of the five available polymerases so that the β-sliding clamp is occupied by high-fidelity polymerases in unperturbed cells, but allows access to TLS polymerases in the event of DNA damage? The high-fidelity polymerases Pols I and III contain high-affinity β-binding motifs and thus preferentially bind the β-sliding clamp over TLS polymerases, which have lower-affinity β-binding motifs [6–8]. Pol I is present at relatively high levels (approximately 400 molecules per cell) [9], which should allow for high rates of binding to β sliding clamps. The main replicative polymerase complex, Pol III holoenzyme, is less abundant. There are 10-20 fully formed Pol III holoenzyme complexes per cell and a small excess of the core sub-complex ($\alpha\epsilon\theta$; $\sim$ 40 molecules per cell) [10]. Within active replisomes, however, Pol III occupies both binding sites on the β sliding clamp through β-binding motifs in its α and ϵ subunits [11]. Copy numbers of Pols II, IV and V are regulated as part of the DNA damage-induced SOS response [12, 13]. Upon damage, levels of Pols II increase from 30 to 350 molecules per cell, and from approximately 200 to 2000 for Pol IV [14, 15]. Pol V is rarely expressed in undamaged conditions and reaches around 100 molecules per cell in UV-irradiated cells [16–18].

Several models have been proposed to describe how high-fidelity DNA polymerases exchange for TLS polymerases in the event of DNA damage. In the 'mass action' model (Fig. 5.1A), TLS polymerases gain increased access to the β-sliding clamp due to the SOS-induced increase in concentration that allows them to more effectively compete with Pols I and III [6, 8, 19]. In the 'traffic cop' model (Fig. 5.1B), polymerase switching depends on whether the upstream single-stranded DNA (ssDNA) is coated by the single-stranded DNA binding protein, SSB, or the recombination/repair protein RecA [20]. In undamaged cells, ssDNA formed by helicase-mediated unwinding in the replisome is quickly coated by SSB, which in turn is rapidly displaced from the template by the advancing replicative Pol III. When the template DNA becomes damaged, Pol III will be blocked and ssDNA per-

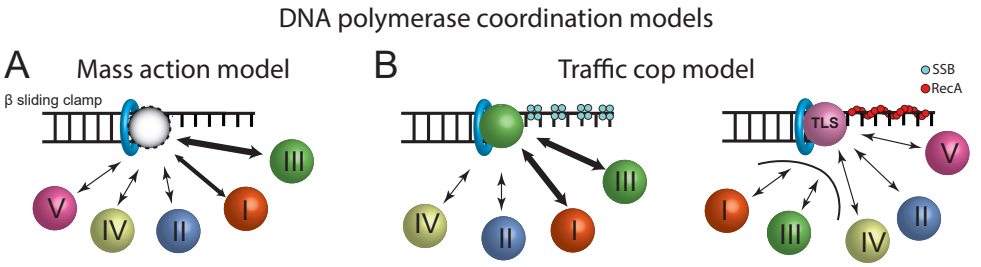

Figure 5.1 | DNA polymerase coordination models. Schematic representation of current models describing the coordination of polymerase binding at the bacterial replication fork and the interactions between DNA polymerases with the β-sliding clamp. A – 'Mass action' model. All the polymerases interact with the β-sliding clamp and polymerase binding controlled by the affinity (K_D) of these interactions and the concentration of each polymerase. B – 'Traffic cop' model. SSB and RecA act as a switch to regulate polymerase occupancy. SSB bound to ssDNA promotes DNA polymerase III activity (I) and inhibits Pol II and Pol IV. Conversely, RecA nucleoprotein filaments have the opposite effect. They inhibit Pol III and promote TLS polymerase occupancy at the replication fork (II).

sists for a longer period of time. In such a scenario, SSB becomes displaced by RecA proteins that bind to the ssDNA and form nucleoprotein filaments. These filaments, denoted as RecA*, serve as substrates for homologous recombination and also induce the SOS response. Importantly, it was recently discovered that RecA* filaments stimulate the activities of TLS polymerases and inhibit the activity of Pol III *in vitro* [20]. Thus, RecA acts like a traffic cop, appropriately directing TLS polymerases to damaged DNA.

The 'mass action' and 'traffic cop' models are not mutually exclusive and the extent of polymerase switching that occurs in cells may actually be a product of the two. In addition, the affinity of each DNA polymerase may vary for different DNA templates, particularly those containing lesions. This difference in affinity might also play a role in selecting which polymerase gains access. It is also worth noting that the relative contribution of these mechanisms may be different for the various types of polymerases. Several studies point to the importance of mass action-driven competition in regulating the activities of Pols II and IV [19, 21–23] but little is known about its effect on Pol V activity.

Relative to the mechanisms governing production and function of Pols II and IV, the regulation of Pol V activity is extremely complex, requiring a series of post-translational modifications before the active form, Pol V Mut, is able to support DNA synthesis [24]. We recently showed that Pol V is also regulated spatially: inactive forms are initially sequestered at the cell membrane, then later released into the cytosol as active Pol V Mut [18]. Until now, the complex regulatory pathways of Pol V, together with its extremely low expression levels, have largely precluded study of how it gains access to DNA. Here we report the use of single-molecule fluorescence imaging of Pol V in live *E. coli* cells to study the relative importance of mass action-driven competition with other polymerases in determining the frequency with which Pol V gains access to damaged and undamaged DNA.

We created mutants of *E. coli* in which replisomes and Pol V are fluorescently

tagged (DnaX-YPet and UmuC-mKate2 respectively) and potential competitors, Pols II and IV, are deleted. We compared levels of Pol V Mut binding to DNA, as well as colocalization of Pol V Mut and replisomes, in the presence and absence of Pols II and IV. We examined Pol V behavior in the context of both UV-damaged wild-type cells and in cells carrying the *recA*(E38K) mutation. This strain constitutively induces high Pol V expression and activity due to formation of RecA(E38K)* filaments, and thus induction of the SOS response, in the absence of DNA damage. Our experiments indicate that in both strains access of Pol V to binding sites on the DNA is not significantly affected by the presence or absence of Pols II and IV. The *recA*(E38K) mutation, on the other hand, has a large effect on the ability of Pol V to access DNA. Our results suggest that for Pol V the 'traffic cop' mechanism dominates over mass action driven competition with other polymerases.

5.2. Results

5.2.1. Single-molecule visualization of polV and the replisome in live *E. coli* cells

In order to visualize the intracellular positions of replisomes and Pol V, we modified *Escherichia coli* K-12 MG1655 cells to produce fluorescent protein fusions. The yellow fluorescent protein YPet was fused to the C-terminus of the DnaX protein, which comprises the τ-subunit of the Pol III holoenzyme and thus acts as a replisome marker [18]. The bright red fluorescent protein mKate2 was fused to the C-terminus of UmuC, a Pol V subunit. Both fusions are functionally active (Robinson et al., 2015). We combined the DnaX-YPet and UmuC-mKate2 fusions with deletions of *polB* (encoding Pol II) or *dinB* (encoding Pol IV), and with the *polB*/*dinB* double deletion. A complete list of strains used in this study is provided in Table 1. We imaged cells using a purpose-built single-molecule fluorescence microscope [18].

5.2.2. Pols II and IV have little effect on the spatiotemporal regulation of Pol V

In our previous work, we used single-molecule microscopy to measure changes in Pol V expression and localization in response to UV-induced DNA damage. We found that when the Pol V subunit UmuC is first produced, some 30-90 minutes after irradiation, it is sequestered at the cell membrane [18]. After a further delay, it is released into the cytosol as part of Pol V Mut. Before we examined the effects of removing Pols II and IV on the ability of Pol V Mut to access DNA, we first wanted to examine if these deletions significantly changed the membrane binding and release behavior of Pol V. We repeated our earlier two-color time-lapse analysis, comparing cells carrying Pols II and IV (*pol*$^+$) with cells lacking both (Δ*polB* Δ*dinB*). We made this comparison in both wild-type *recA*$^+$ and hypermutagenic *recA*(E38K) cells. To visualize the behavior of the fluorescently labeled Pol V and replisomes within these strains, we introduced *E. coli* cells to a microfluidic structure designed for long-time fluorescence imaging. We irradiated with UV light (fluence = 10 J.m^{-2}, λ = 254 nm)

and produced time-lapse series by capturing images every five minutes for a total of three hours.

Visual inspection of the time-lapse movies (Fig. 5.2) revealed the expected up-regulation of UmuC-mKate2 and changes in its localization behavior. For both *pol*$_+$ *recA*$_+$ and Δ*polB* Δ*dinB recA*$^+$ cells, UmuC-mKate2 up-regulation could be observed around 60 minutes after UV damage. Clear signals for membrane-associated UmuC-mKate2 were visible for both strains, consistent with our earlier observations [18]. For the *recA*(E38K) variants, we observed elevated UmuC-mKate2 signals prior to UV damage, also as observed previously [18]. Further, these strains showed reduced association of UmuC with the cell membrane, characteristic of *recA*(E38K) strains. No clear differences could be observed between *pol*$^+$ *recA*(E38K) cells and Δ*polB* Δ*dinB recA*(E38K) cells. Thus, our initial results suggested that deleting Pols II and IV had little influence on Pol V regulation.

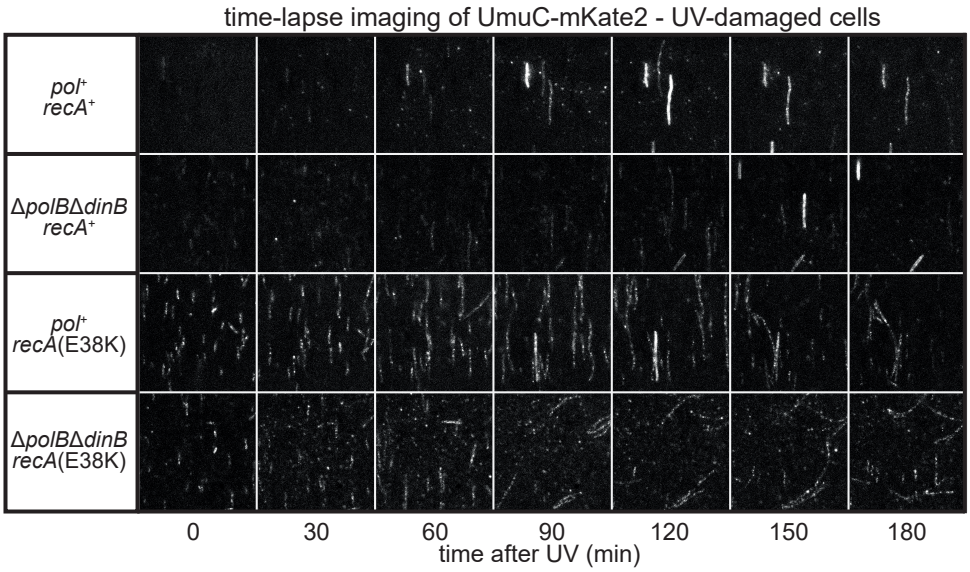

Figure 5.2 | Monitoring UmuC-mKate2 expression upon UV-based DNA damage. Time-lapse imaging of *E. coli* K-12 MG1655 containing UmuC-mKate2 chromosomal fusion. *Pol*$^+$ indicates that all polymerases genes are present; polymerase deletions are indicated where necessary. The genetic modification of recA to *recA*(E38K) was combined with the presence or absence of different polymerase as indicated. Cells were grown at 37 °C in flow cells and irradiated in situ with 10 J.m^{-2}of UV light (λ = 254 nm). Following UV irradiation, fluorescence images were recorded every five minutes for three hours. These images reveal that UmuC induction begins between 30-60 minutes in *recA*$^+$ background while *recA*(E38K) shows constitutive UmuC-mKate2 expression.

s

As a next step, we used our recently described localization tool (J.M.H. Goudsmits *et al*, under review with Biophysical Journal) to characterize the intracellular distribution of Pol V (UmuC-mKate2) and subsequent redistribution upon DNA damage. This tool allows for averaging of fluorescence signals from multiple cells and is particularly useful for analysis of single-molecule images where signals are often

sparsely distributed within cells. The work flow is summarized in Fig. 5.3A. Bright-field images are subdivided into tiles containing a single cell or fragment thereof (Fig. 5.3A-I). Cell fragments are aligned along the vertical axis of the tile (Fig. 5.3A-II) and then centered (Fig. 5.3A-III). Using the transformation parameters determined from the bright-field images, the fluorescence signals from cell fragments are overlaid and averaged (Fig. 5.3A-IV). The averaged fluorescence signals are then projected to a line scan that describes the average distribution of fluorescence across the short axis of the cell. Membrane-associated signals produce two distinctive peaks at ±0.5 µm, whereas cytosolic/nucleoid associated signals produce a broader peak, centered at 0 µm. The process is repeated for all time points in a time-lapse series and the resulting line scans are plotted as a function of time, producing 2D contour plots.

We calculated the line scans for the time-lapse data shown in Fig 5.2. A total of 120 fields of view were analyzed, corresponding to approximately 2400 cells. As expected, *pol*$^+$ *rec*A$^+$ cells showed a clear increase in UmuC-mKate2 signal, beginning approximately 60 minutes after UV damage. These cells displayed predominantly membrane-associated signatures, consistent with membrane sequestration of UmuC-mKate2 [18] . The relative contributions of membrane-associated and cytosolic Pol V foci can be quantified by fitting each line scan with linear combinations of profiles from known membrane and cytosolic proteins. As expected, the amount of Pol V entering the cytosol increases towards the end of the measurement, as membrane-sequestered UmuC is released into the cytosol as activated Pol V Mut (Fig. 5.3B; [18](J.M.H. Goudsmits, under review with Biophysical Journal)).

Cells lacking both Pol II and Pol IV (Δ*polB* Δ*dinB* *recA*$^+$) showed similar up-regulation of UmuC-mKate2 and membrane-associated signatures (Fig. 5.3C) as *pol*$^+$ cells (Fig. 5.3B). Thus, deleting the genes encoding Pols II and IV had little or no effect on the damage induced up-regulation or localization behavior of Pol V in the wild-type *recA*$_+$ background. We then repeated our analysis for *recA*(E38K) cells. As observed previously [18], *pol*$^+$ *recA*(E38K) cells produced significant amounts of UmuC-mKate2 in the absence of DNA damage and generated a strong cytosolic/nucleoid-associated signature (Fig. 5.3D). Levels of UmuC-mKate2 remained high after UV irradiation, with a mild increase in membrane-associated signatures, consistent with our earlier analyses. Cells lacking Pol II and Pol IV (Δ*polB* Δ*dinB* *recA*[E38K]) again showed little difference from *pol*$^+$ cells (Fig. 5.3E). Overall, our time-lapse analyses indicate that deletion of Pols II and IV has little effect on the damage-induced up-regulation of Pol V, or its localization behavior.

5.2.3. Removal of Pols II and IV has little effect on Pol V Mut binding at replisomes

Our previous work demonstrated that Pol V Mut molecules bound to DNA produce static UmuC-mKate2 foci within the nucleoid region of the cell [18]. Contrary to expectation, we found that these Pol V Mut foci did not colocalize with replisome foci, conflicting with the long-standing model that Pol V-catalyzed TLS occurs at replisomes that have stalled at damage sites. In contrast, we found that Pol V

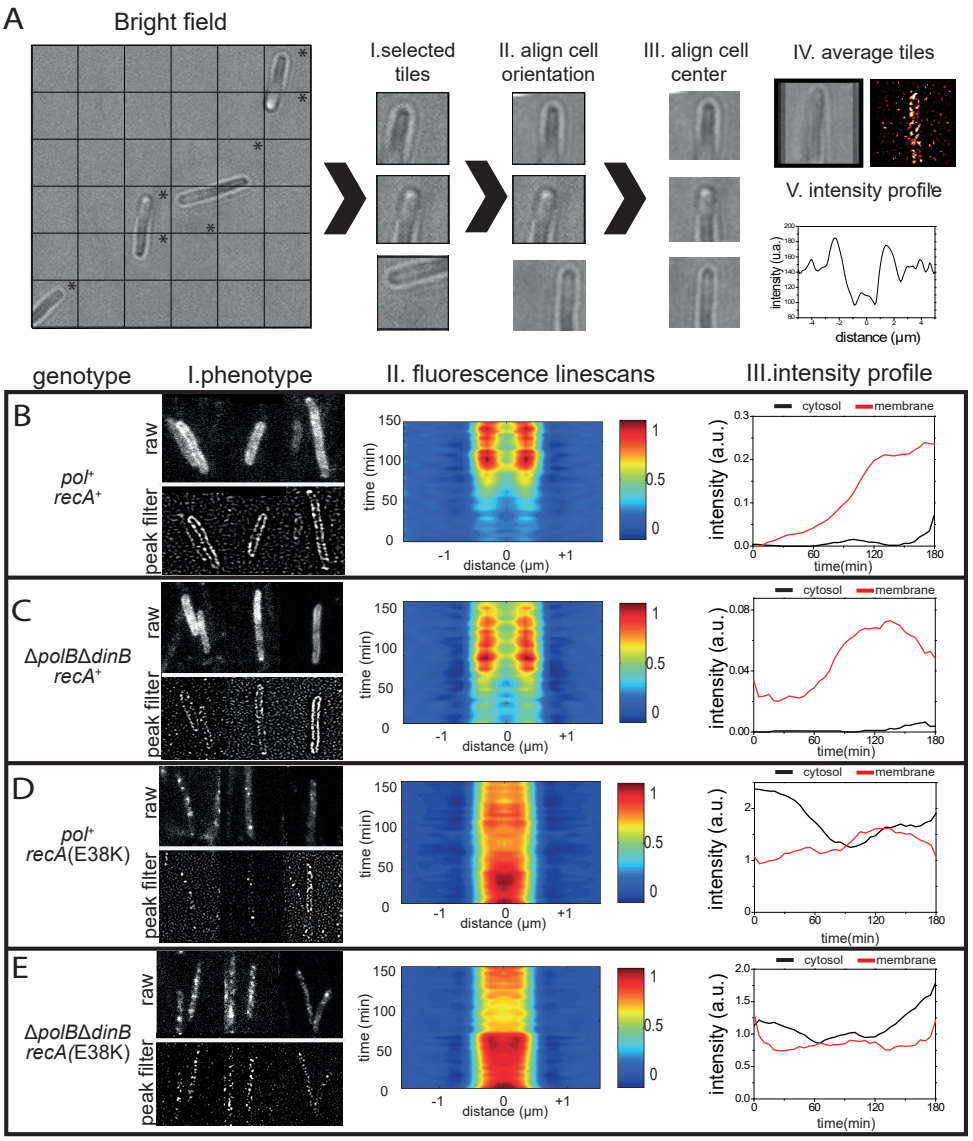

Figure 5.3 | Intensity linescans of DNA polymerase foci upon UV-based DNA damage. Full caption on the next page.

Mut foci did colocalize with replisome foci in the mutant *recA*(E38K) background. These observations could be explained in two ways. In line with the mass action model (Fig. 5.1A), Pol V Mut might be physically capable of binding at replisomes in *recA*$^+$ cells, but is out-competed by Pols II and IV. The increased levels of Pol V Mut present in the *recA*(E38K) background might then allow for more effective competition and thus increased colocalization. Alternatively, considering the traffic

Figure 5.3 | Intensity linescans of DNA polymerase foci upon UV-based DNA damage. A – Determination of average fluorescence line scans. Bright-field images are used as the spatial reference to align the fluorescence images. I. Bright-field images are subdivided in tiles (I) and the tiles with cellular features are selected (tiles with * - II). Cells are then oriented along their long axis (III) and centred within the tile (IV). An average of all valid tiles is calculated for the fluorescence channels by taking the bright field as a reference. The fluorescence signal is projected in the horizontal axis and the profile obtained (V) represents a particular data point in the experiment. A peak enhancer algorithm was applied prior to the intensity calculation [25]. B-E – Temporal evolution of UmuC-mKate 2 fluorescence intensity line scans. (I) Example cells originating from average projections of UmuC-mKate2 images. (II) The spatiotemporal behaviour of UmuC-mKate2 is summarized in heatmaps containing fluorescence linescans obtained as a function of time for a particular strain or condition. The center of the heatmap corresponds to the center of the center of a cell. Cells were damaged with UV at time zero (fluence = 10 $J.m^{-2}$, λ = 254 nm). In *recA*$^+$, UmuC-mKate2 is localizing to the cellular membrane (sharp lines around $\pm$0.6 µm) while in the *recA*(E38K) background UmuC-mKate2 foci are found distributed throughout the whole cell. (III) Total fluorescence signal found at the cellular membrane or in the cytosol. RecA$^+$ strains show total fluorescence increasing upon UV damage. For this strain, UmuC-mKate2 foci is mainly found at the cellular membrane. For RecA(E38K) strains, UmuC-mKate2 is constitutivelly expressed, resulting in higher levels throughout the experiment.

cop model, colocalization may be driven by the formation of RecA(E38K)* filament at replisomes. In the wild-type background, RecA* filaments may not form close to replisomes, but instead form on ssDNA gaps left behind replisomes that skip over damage sites [26]. These RecA* filaments would direct Pol V Mut to bind at sites left far behind the replisome, leading to little colocalization. RecA(E38K) competes far more effectively with SSB for binding to ssDNA than wild-type RecA and thus RecA(E38K)* filaments frequently form on the lagging strand, even in the absence of DNA damage [27]. Pol V Mut would be directed to these lagging-strand RecA(E38K)* filaments, producing significant levels of colocalization. Our previous analyses showed that in *recA*(E38K) cells, levels of colocalization decreased in response to UV irradiation as new binding sites for Pol V Mut formed at sites away from replisomes. This observation is difficult to explain in light of the mass action model and is more compatible with the 'traffic cop' explanation.

To examine this phenomenon further, we measured levels of colocalization between Pol V Mut and replisomes in the presence and absence of Pols II and IV. If binding of Pol V Mut is disfavored at replisomes because Pol V Mut is not able to effectively compete with Pols II and IV, we would expect that Pol V Mut might show increased colocalization with replisomes in the absence of Pols II and IV. In the *recA*(E38K) background, colocalization would also be expected to increase in the absence of Pols II and IV. On the other hand, if Pol V Mut binding is directed by RecA* filaments, i.e. if the traffic cop model applies, colocalization would be predicted to be similar in both the presence and absence of Pols II and IV.

We analyzed colocalization between Pol V Mut and replisomes in two different ways. Time-dependent changes in colocalization throughout our time-lapse data were measured globally (across all cells) using a cross-correlation approach. More precise measurements were then made at the level of single foci by analyzing high time-resolution, short-duration movies (total duration 3.4 seconds, 100 frames) taken either 60 min after UV irradiation (*recA*$^+$ cells) or without irradia-

tion (*recA*[E38K] cells). The cross-correlation approach is based on the line-scan analysis described earlier (Fig 5.3A). Having aligned and centered cell fragments identified within time-lapse images, we calculated the cross-correlation functions of DnaX-YPet and UmuC-mKate2 line scans. We expected that cell fragments containing colocalized peaks would return cross-correlation functions with a strong, narrow peak at 0 µm. Assuming perfect alignment of cell fragments, the width of this peak should correspond to the diffraction limit (FWHM ∼0.3 µm). Conversely, cell fragments containing non-colocalized peaks are expected to produce cross-correlation functions with a broader, weaker peak at 0 µm. The width of this peak should correspond to the average width of the cells (FWHM ∼1 µm). As a positive control, we applied our cross-correlation approach to time-lapse images of cells in which the τ and ϵ subunits of Pol III holoenzyme were tagged with yellow and red fluorescent proteins respectively (DnaX-YPet, DnaQ-mKate2). As expected, DnaX-YPet and DnaQ-mKate2 foci showed a high degree of colocalization (Fig. 5.4A). Correspondingly, the time-dependent cross-correlation function showed a strong, sharp peak. As a negative control, we randomized the table of DnaQ-mKate2 line scans prior to measuring the cross-correlation against DnaX-YPet line scans. In this way, line scans from distinct, spatially unrelated cell fragments were compared. Because each cell fragment is aligned and centered before analysis, this approach is similar to comparing non-colocalized signals within the same cell. As expected, this randomized data set produced a cross-correlation function with a broad, weak peak. Both these positive and negative controls verify our approach based on the calculation of the spatial cross correlation. Further, the cross-correlation function derived from the randomized data is indicative of the baseline levels of accidental colocalization that arise due the signals being confined within cells of regular width.

Applying our cross-correlation approach to the DnaX-YPet/UmuC-mKate2 strains, we observed that deleting the genes for Pol II, Pol IV or both, had little effect on the colocalization of Pol V with replisomes (Fig. 5.4C). All four *recA*$^+$ strains produced cross-correlation versus time plots that show a broad, weak peak centered at 0 µm, indicative of little or no colocalization between Pol V and replisomes. In no case did the removal of Pols II and/or IV significantly increase colocalization of Pol V with replisomes. The minor differences observed between strains most likely arise from experimental variation. The cross-correlation peaks obtained for DnaX-YPet/UmuC-mKate2 cells were noticeably broader than those corresponding to the randomized DnaX-YPet/DnaQ-mKate2 control due to the abundance of membrane-associated signals in the former. All four *recA*(E38K) strains produced cross-correlation functions with a strong and sharp peak, indicative of colocalization of Pol V with replisome foci. This observation is consistent with our previous measurements in which the *recA*(E38K) mutation was found to significantly enhance co-localization [18]. As observed for the *recA*$^+$ background, removing Pols II and/or IV in the *recA*(E38K) background did not lead to increased colocalization between Pol V and replisomes. Overall, our time-lapse/cross-correlation analyses showed similar behavior to that observed in previous measurements: Pol V rarely colocalizes with replisomes in the wild-type *recA*$_+$ background, but frequently colocalizes with replisomes in the *recA*(E38K) mutant background. Removal of Pols II or IV has little or no effect on

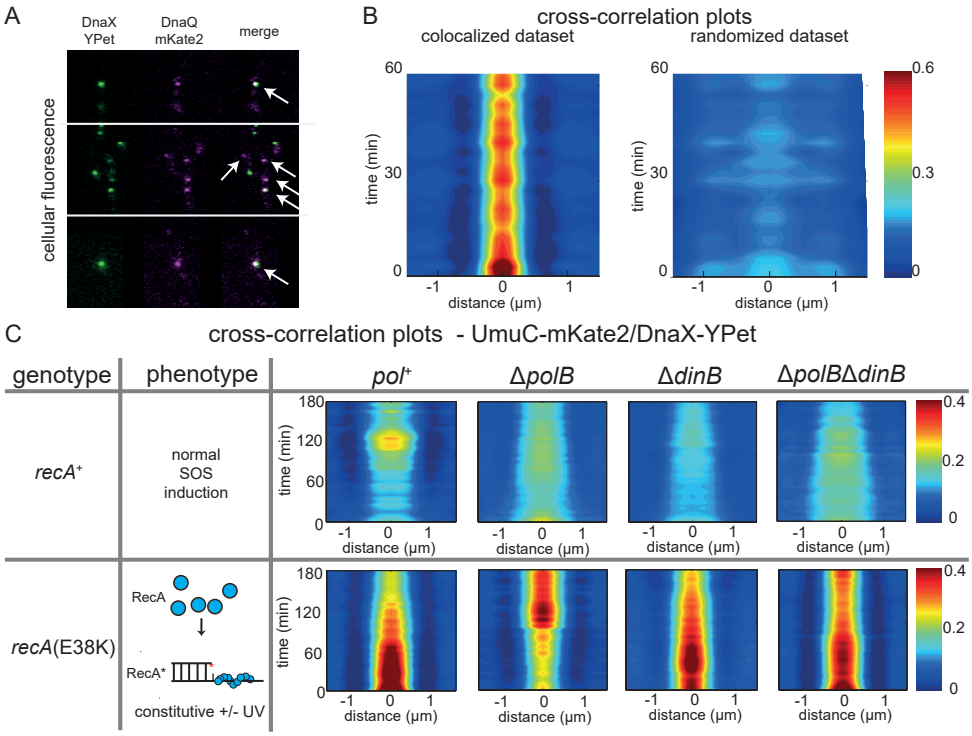

Figure 5.4 | Cross-correlation between UmuC-mKate2 and DnaX-YPet. A – DnaX-YPet and DnaQ-mKate2 fluorescence images and merged channels to illustrate foci colocalization. White arrows point to co-localized foci. B – Cross-correlation images for DnaX-YPet and DnaQ-mKate2 signals. Co-localized foci appear as centralized regions with high contrast. Randomizing the DnaQ-mKate2 / DnaX-YPet image pairing results in non-colocalized peaks and is expressed as a diffused signal. C – Cross-correlation plots of time-lapse images for diferent strains. Cells were damaged with UV immediately after the first time point (t = 0 min). For each series (*recA*$_+$ and *recA*(E38K)) different combinations of polymerase deletions are displayed. In the top row, normal SOS response results in little cross correlation beween the replisome (DnaX-YPet) and Pol V (UmuC-mKate2). Below, *recA*(E38K) cells display higher contrast, indicating higher co-levels of localization between Pol V and the replisome. The plot for the Δ*polB recA*(E38K) strain shows low initial levels of cross-correlation due to surface artifacts giving rise to an decreased UmuC-mKate2 signal-to-noise ratio during the first 90 minutes.

Pol V-replisome colocalization.

To determine whether Pols II and IV had a more subtle effect on Pol V-replisome colocalization, we measured colocalization at the level of single foci. Here, cells were sampled from shaking culture as opposed to imaging with flow cells. Wild-type *recA*$^+$ cells were irradiated with 10 J.m^{-2}UV light and incubated for 60 min prior to imaging to allow for expression of UmuC-mKate2 and activation to Pol V Mut. Mutant *recA*(E38K) cells, in which Pol V Mut is produced constitutively, were imaged without exposure to UV light. Rather than recording individual snapshots, as was the case with the time-lapse analysis described above, short movies of UmuC-mKate2 fluorescence were recorded at high time resolution to aid in iden-

tifying Pol V Mut molecules bound to DNA. These DNA-bound molecules remain relatively static through the movies and thus appear in the movies as spots that show little movement. Averaging all the frames within such a movie would give rise to bright, punctate foci. In contrast, molecules diffusing along the cell membrane or throughout the cytosol tend to blur out in average projections. In this way, DNA-bound molecules can be selected over non-DNA bound molecules by scoring bright, punctate foci in average projections of movies. The number of static foci per cell and the proportion that colocalize with replisome foci could then be quantified on a cell-by-cell basis (Fig. 5.5A).

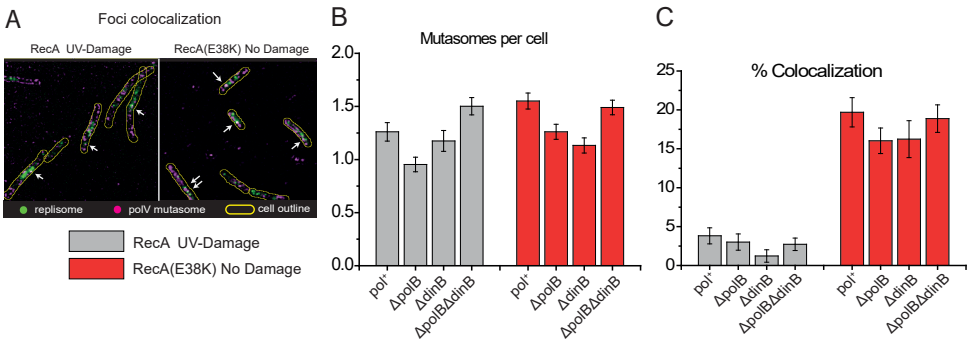

Figure 5.5 | Colocalization of replisomes and mutasomes. A – Average projections of UmuC-mKate2 (Pol V mutasomes) superimposed with DnaX-YPet (replisomes). Left panel contains wild-type (EAW282) cells after 60 minutes of UV damage (fluence = 10 J.m^{-2}, λ = 254 nm) and the right panel contains *recA*(E38K) cells (EAW307) in the absence of UV damage. Arrows indicate mutasome-replisome co-localized pairs. Cellular outlines (yellow) were used for quantification of replisome-mutasome pairs for each strain. B – Number of mutasome foci per cell. Error bars indicate standard error of the mean. Datapoints are grouped into *recA*$_+$ and *recA*(E38K) background with diffent polymerase deletions. For *recA*$^+$ bakground (gray): no deletion (EAW282, n_{cells} = 230), Δ*polB* (EAW330, n_{cells} = 216), Δ*dinB* (EAW331, n_{cells} = 177) and Δ*polB*Δ*dinB* (EAW337, n_{cells} = 305). For *recA*(E38K) bakground (red): no deletion (EAW307, n_{cells} = 296), Δ*polB* (EAW332, n_{cells} = 341), Δ*dinB* (EAW333, n_{cells} = 196) and Δ*polB*Δ*dinB* (EAW341, n_{cells} = 347). The statistical significance of the differences between strain pairs is provided as a supplement (Table S1). C – Percentage of mutasome colocalized with replisomes. The percentage was determined per cell and then averaged. Error bars indicate standard error of the mean. Pols II and IV do not show significant differences between each strain (Table S2).

We found that *recA*$^+$ cells contain a similar number of static Pol V foci (1.2 ± 0.1 per cell on average; 1,312 cells) in the presence and absence of Pols II and IV. The mean values were found not to be significantly different between strains (Supplementary Table 1). Similar results were found for the *recA*(E38K) background: cells contained 1.3 ± 0.1 Pol V Mut foci per cell (1,180 cells) and removal of Pols II and/or IV did not produce significant differences from the *pol*$^+$ cells. Our analysis therefore indicated that the presence or absence of Pols II and IV has little effect on the number of Pol V molecules that bind to DNA at any particular time. In order to determine whether Pols II and IV affected the proportion of Pol V Mut molecules that bound at replisomes versus other sites on the DNA, we next measured the proportion of Pol V Mut foci that colocalized with replisomes. A Pol V Mut focus was designated as colocalized if its fitted centroid position fell within 200 nm of

a replisome focus. In the *recA*$^+$ background, colocalization was uniformly low (2-4%) for all four strains, within levels expected to occur by chance (~ 5%; [18]. No significant difference was found between the strains. In the *recA*(E38K) background, colocalization was uniformly high (17-20%), with no significant differences between strains containing or lacking Pols II and/or IV. Taken together, our single focus analyses support our time-resolved analyses and indicate that Pols II and IV have no effect on the number of Pol V Mut molecules that act on DNA, nor on the tendency of Pol V Mut to bind at replisomes.

5.3. Discussion

In this work, we found that Pols II and IV do not significantly affect the upregulation, membrane sequestration or the number of binding sites available for Pol V on the DNA. Our results suggest that competition driven by mass action plays little or no role in the regulation of Pol V Mut activity on the DNA. Conversely, our data strongly support a role for RecA* as a 'traffic cop', directing Pol V Mut binding to DNA. By effectively competing with SSB for ssDNA formed at replication forks, RecA(E38K) allows Pol V Mut to access replisomes (Fig. 5.6B). This behavior does not take place with wild-type RecA, which is less able to compete with SSB and thus forms nucleoprotein filaments much more slowly. Accordingly, Pol V-dependent mutagenesis is 100-fold higher in *recA*(E38K) cells than wild-type cells [28]. Upon UV irradiation, a replisome encountering damage is able to skip over the lesion [26], thus leaving a ssDNA gap. This gap is eventually coated with RecA and becomes a potential substrate for Pol V Mut (Fig. 5.6C-D).

It is important to note that in this study we only investigated Pol V behavior under the conditions of UV-induced damage and in the *recA*(E38K) background. It is possible that Pols II and IV do affect Pol V behavior under different conditions, particularly in the presence of lesions favored by Pols II and IV. The potential for the chemical nature lesions to play a role in selecting which DNA polymerase bind and carry out TLS remains a fascinating area of research. It is also important to note that in the current study we were able to measure only the number of available binding sites for Pol V Mut on the DNA. It is possible that rather than occluding binding of Pol V Mut altogether, Pols II and IV affect the frequency of Pol V Mut binding at binding sites, thus regulating its activity kinetically as opposed to thermodynamically. Even though analysis of binding kinetics of proteins in live cells is possible using single-molecule imaging, this approach is technically challenging due to photophysical limitations of currently available fluorescent proteins. Rapid advances in the development of more photostable fluorescent probes suggest that a full kinetic analysis of the recruitment of TLS polymerases at sites of replication may soon be within reach. Our study highlights the utility of single-molecule fluorescence measurements in measuring the properties of DNA-binding proteins in live cells and demonstrates the strength of these approaches in obtaining quantitative information and mechanistic insight.

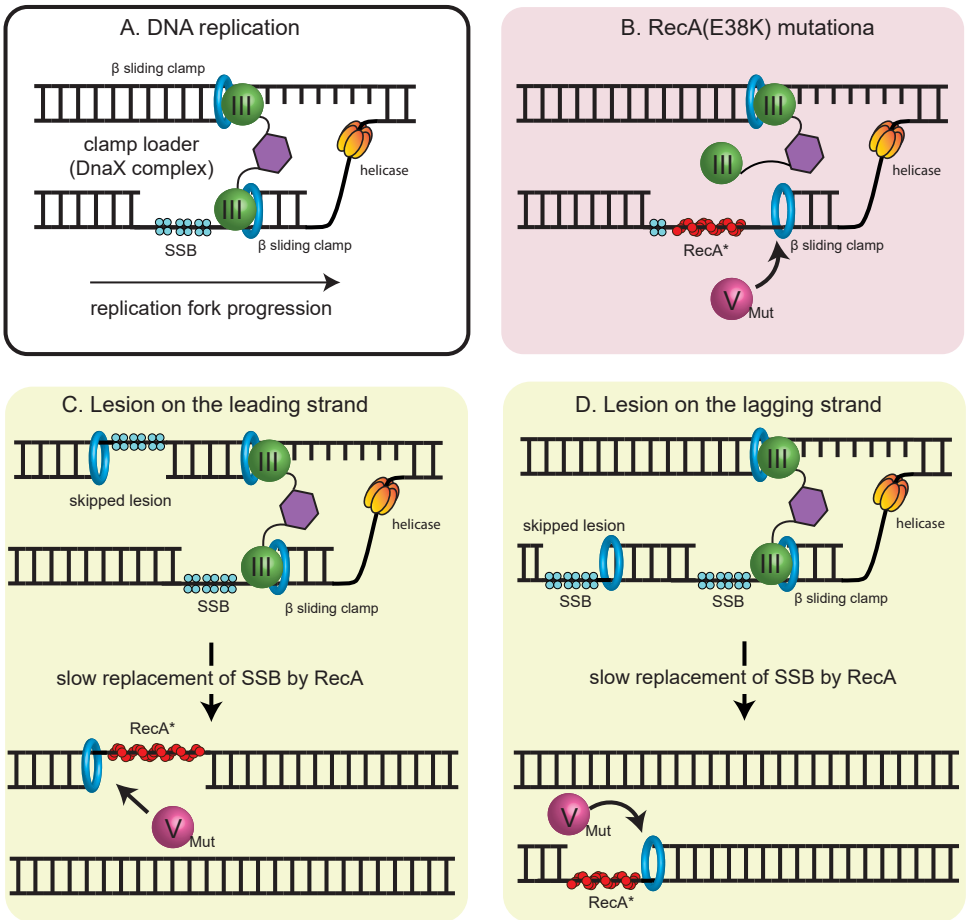

Figure 5.6 | DNA Polymerase V and DNA damage. A – Schematic representation of DNA replication occuring without disruption by lesions on the DNA template. Leading-strand DNA synthesis occurs on DNA continuously while the lagging strand is produced in a discontinuous fashion. DnaB helicase unwinds dsDNA ahead of the replisome and SSB binds to ssDNA on the lagging strand. B – RecA(E38K) mutants displace SSB. The formation of RecA* facilitates Pol V binding to the β-sliding clamp and promotes error-prone DNA synthesis. C-D – Pol III HE encounters a lesion on the DNA template and skips over the lesion leaving behind an assembled β-sliding clamp and a ssDNA gap. SSB is then substituted by RecA, forming RecA* nucleoprotein filaments, and Pol V is recruited for DNA synthesis.

5.4. Experimental procedures

Construction of strains

A complete list of *Escherichia coli* strains used in this study is provided in Table 5.1. EAW18 and EAW21 strains are both *E. coli* K-12 MG1655 derivatives [29]. The strains were constructed using a modified version of the λ RED recombination system [30, 31]. The plasmid pEAW507 contains a mutant FRT-Kan^R-wtFRT cassette

Table 5.1 | Strains used in this study

Strain	Relevant Genotype	Parent strain	Source/technique
MG1655	*recA*$^+$ *sulA*$^+$ *polB*$^+$ *dinB*$^+$ *umuC*$^+$	-	[29]
EAW18	Δ*dinB*	MG1655	λ RED recombination
EAW21	Δ*polB*	MG1655	λ RED recombination
EAW191	*umuC*-mKate2	MG1655	[18]
EAW282	*dnaX*-YPet *umuC*-mKate2	JJC5945	[18]
EAW288	*sulA*$^-$ *recA*(E38K) *umuC*-mKate2	EAW297	[18]
EAW307	*sulA*$^-$ *recA*(E38K) Δ*dinB* *umuC*-mKate2 *dnaX*-YPet	EAW288	transduction to Δ*dinB* with P1 grown on JJC5945
EAW330	Δ*polB* *umuC*-mKate2 *dnaX*-YPet	EAW282	transduction to Δ*polB* with P1 grown on EAW21
EAW331	ΔdinB *umuC*-mKate2 *dnaX*-YPet	EAW282	transduction to Δ*dinB* with P1 grown on EAW18
EAW332	*sulA*$^-$ *recA*(E38K) Δ*polB* *umuC*-mKate2 *dnaX*-YPet	EAW307	transduction to Δ*polB* with P1 grown on EAW21
EAW333	*sulA*$^-$ *recA*(E38K) Δ*dinB* *umuC*-mKate2 *dnaX*-YPet	EAW307	transduction to Δ*polB* with P1 grown on EAW18
EAW337	Δ*pol* Δ*dinB* *umuC*-mKate2 *dnaX*-YPet	EAW330	transduction to Δ*dinB* with P1 grown on EAW18
EAW341	*sulA*$^-$ *recA*(E38K) Δ*polB* Δ*dinB umuC*-mKate2 *dnaX*-YPet	EAW332	transduction to Δ*polB* with P1 grown on EAW18

in an ampicillin backbone. The gene knockouts were made by replacing *dinB* (in the EAW18 strain) and *polB* (in the EAW21 strain) genes in the native chromosome by FRT cassette following a protocol previously described [32]. Transformed strains were plated on LB-agar, supplemented with 40 μg ml^{-1} of kanamycin and grown overnight. Kanamycin-resistant strains were further screened for ampicillin resistance. EAW18 and EAW21 were used as donor strains for p1 transduction. Strains EAW307, EAW330-3, EAW337 and EAW341 were made by p1 transduction [33] in one or more steps as inferred from Table 5.1. P1 transduction of donor strain to the desired genotype was performed growing P1 bacteriophage on the source strain. Mutants were selected by kanamycin resistance and screened for chloramphenicol sensitivity.

Fluorescence microscopy

The experiments were performed in a home-built wide-field single-molecule fluorescence microscope, consisting of an Olympus IX-81 microscope body equipped with a 1.49 NA 100x objective and a 512 × 512-pixel EM-CCD camera (C9100-13, Hamamatsu). To image DnaX-YPet, we used a continuous-wave optically pumped semiconductor 514-nm laser (150 mW maximum output, Sapphire LP, Coherent). Samples were excited with light at 10 W.cm^{-2}and emitted light was collected be-

tween 525-555 nm (ET540/30m filter, Chroma). For imaging UmuC-mKate2, we use a 568-nm wavelength laser (200 mW max. output, Sapphire LP, Coherent). For this particular fluorescent protein, we use a higher excitation intensity (180 W.cm^{-2}) and collected light emitted between 610-680 nm (ET 645/75m filter, Chroma). ImageJ extended with iSBatch plugin [34, 35] was used for image analysis. Individual cellular outlines were assigned using MicrobeTracker [36] and converted to ImageJ regions of interest (ROI) by iSBatch [35].

Time-lapse fluorescence microscopy setup and imaging

For time-lapse experiments we used a flow-cell design previously described [18, 37]. In brief, the device is a custom flow cell assembled with a quartz top for in situ UV irradiation and a cover slip treated with 3-aminopropyl triethoxy silane (APTES, Sigma) as the bottom. Top and bottom are connected using double-sided tape (3M) and the device is sealed with epoxy resin. The channel dimensions are 3 x 30 x 0.03 mm (length x width x height) and growth medium flows in and out via polyethylene tubes (PE-60, Bioseb). We mounted the flow cells to the microscope, maintaining the temperature at 37 ˚C by a combination of stage heating and objective lens heating. Cell cultures grown overnight were diluted 1:100 in EZ rich medium (Teknova) and grew until mid-log phase ($OD_{600} \sim 0.5$). Cells were then loaded into flow cells by pulling gently with a syringe and were allowed to sit for 2 minutes. The single inlet was then placed into fresh medium that was constantly aerated using an aquarium pump. Medium was then pulled through the flow cell using a syringe pump, at a rate of 30 µL/min . Cells were irradiated in situ with 254-nm UV light from a mercury lamp (UVP) at a fluence of 10 J.m^{-2}. First image was taken before damage and followed by acquisition for 180 minutes after UV damage at five-minute intervals. Each imaging time point contains a 514-nm image (DnaX-YPet), a 568-nm one (DnaX-YPet) and a bright-field image. The following imaging conditions apply: Bright-field image was acquired with 50 ms acquisition time; DnaX-YPet and UmuC-mKate2 each with 50 ms acquisition time at 180 W.cm^{-2}.

Time-sampling fluorescence microscopy cells grown in shaking culture

Cells were grown in shaking culture at 37 ˚C in EZ rich defined medium (Teknova) supplemented with 0.2% (w/v) glucose. To induce DNA damage, cells were grown until mid-log phase ($OD_{600} \sim 0.5$), placed between two quartz sheets separated by 170-µmspacers and irradiated with 254-nm UV light from a mercury lamp (UVP) at a fluence of 10 J.m^{-2}. Cells were then put back into shaking culture in preparation for imaging.

Microscopy samples were prepared by transferring 30 µLof cll suspension onto a coverslip treated with 3-aminopropyl triethoxy silane (APTES, Sigma) and placing a clean coverslip on top. Cells were allowed to settle for 1-2 min and excess medium was removed by gently pressing down on the top coverslip. The device was placed in the microscope maintaining the temperature at 37 ˚C by a combination of stage heating and objective lens heating. Imaging started within 3 min after loading the sample in the coverslip. For each coverslip, 10 different FOVs were imaged, taking a maximum of 10 min total time per coverslip. Cells grew and divided at similar rates

before and after imaging, indication no disturbance in the cell cycle caused by the laser or the device. Each region (FOV) was imaged only once, with the following conditions: a bright-field image consisted of a single frame of 50 ms acquisition time. The DnaX-YPet channel contained a single frame of 500 ms acquisition time at 1800 W.cm^{-2} (excitation) and the UmuC-mKate2 image was obtained by exciting at 180 W.cm^{-2} and acquiring 100 frames of 34 ms each.

Image pre-processing
All images from the time-lapse or time-sampling acquisitions were initially processed in the same manner before subsequent analysis. This process includes the following steps: subtract the raw image by a background image containing information on the electronic camera offset, divide it by a normalized background image containing information on the excitation profile, and finally subtract a background image that contains information of background fluorescence from the glass and other contributions. The result is a flat and clean image with no background that preserves the intensity range of values.

Analysis of fluorescent protein distribution by autocorrelation and cross-correlation
Fluorescent protein distribution in time-lapse imaging. To analyse the distribution of UmuC-mKate2 in time-lapse experiments we calculate 2D contour plots composed of line scans across the long axis of the cell; each line scan represents one time point. To obtain each line scan, a bright field was subdivided into regions and the regions containing cellular features were selected (Fig. 5.3). Regions without cells were discarded. Tiles containing cells were then rotated to align the cellular long axis to the vertical axis and further centralized in the image tile. For the fluorescence channels, an enhancing filter was applied to the fluorescence channel [25] and the same rotational and translational image operations were then repeated for the fluorescence channels. All valid tiles were averaged and the intensity projected in a 1D array of values to produce a fluorescence line scan. The process was repeated for each time point, resulting in a 2D contour plot representing cellular localization of UmuC-mKate2. The software will be soon available (J.M.H. Goudsmits *et al*, under review with Biophysical Journal).

Time-lapse cross-correlation analysis
Using the line scans representing the cellular distribution of fluorescence, we calculated the cross-correlation functions between UmuC-mKate2 and DnaX-Ypet. Cross correlation was measured over a 1.5 μm distance lag range (15 pixels), with the centre (0 μm) of each cross-correlation contour plot representing no shift between line scans. DnaX-YPet and UmuC-mKate2 fluorescence intensities were used as input and no intensity-based normalization was performed. When reaching the limits of the cellular width (near $\pm$ 0.6 μm), a clear drop in the cross-correlation values is expected. All correlations were measured using the **xcorr** function in Matlab. These cross-correlation functions were plotted as a function of time after UV exposure as a 2D contour plot.

Time-sampling image analysis

In order to identify UmuC-mKate2 foci, the visualization of long-lived, bound molecules was performed by averaging 96 rapid-acquisition frames. Single-molecule foci were identified by applying a discoidal averaging filter [25] to the resulting images and the peaks above a defined threshold value were selected. With a list of peak localizations, each focus on the original images was fitted with a 2D Gaussian function in order to accurately determine their centre positions (non-linear least squares fitting with Levenberg-Marquadt algorithm). Using a custom-developed extension to MicrobeTracker [36], each peak was assigned to a detected cell, including the peak relative position to the cell outline. The list containing all peaks with their respective information was used for further quantification analysis using the statistical package R [38].

5.5. Supplementary information

Table S1 | P-values for number of Pol V Mut foci per cell, comparing pairs of strains. Lower values indicate more certainty in a difference between the means of the number of foci for the two strains.

	Δ*polB* Δ*dinB* *recA*(E38K)	Δ*polB* Δ*dinB* UV	Δ*dinB* *recA*(E38K)	Δ*dinB* UV	Δ*polB* *recA*(E38K)	Δ*polB* UV	*pol*$^+$ *recA*(E38K)	*pol*$^+$ UV
Δ*polB* Δ*dinB* *recA*(E38K)	1							
Δ*polB* Δ*dinB* UV	9.12E-01	1						
Δ*dinB* *recA*(E38K)	3.22E-04	6.78E-04	1					
Δ*dinB* UV	8.87E-03	1.07E-01	7.58E-01	1				
Δ*polB* *recA*(E38K)	2.04E-02	2.60E-02	2.01E-01	4.78E-01	1			
Δ*polB* UV	4.79E-08	3.57E-07	7.03E-02	6.50E-02	1.91E-03	1		
pol$^+$ *recA*(E38K)	5.57E-01	6.58E-01	6.24E-05	2.56E-03	5.24E-03	8.04E-09	1	
pol$^+$ UV	3.90E-02	4.36E-02	2.54E-01	5.14E-01	9.99E-01	5.75E-03	1.21E-03	1

Table S2 | P-values for percentage of Pol V Mut foci colocalization with replisome foci, comparing pairs of strains. Lower values indicate more certainty in a difference between the means of colocalization values for the two strains.

	Δ*polB* Δ*dinB* *recA*(E38K)	Δ*polB* Δ*dinB* UV	Δ*dinB* *recA*(E38K)	Δ*dinB* UV	Δ*polB* *recA*(E38K)	Δ*polB* UV	*pol*$^+$ *recA*(E38K)	*pol*$^+$ UV
Δ*polB* Δ*dinB* *recA*(E38K)	1							
Δ*polB* Δ*dinB* UV	8.61E-16	1						
Δ*dinB* *recA*(E38K)	0.37270	1.58E-07	1					
Δ*dinB* UV	2.20E-16	0.18590	7.11E-09	1				
Δ*polB* *recA*(E38K)	0.23710	1.20E-12	0.94130	4.07E-15	1			
Δ*polB* UV	5.57E-14	0.83070	6.20E-07	0.17710	5.44E-11	1		
pol$^+$ *recA*(E38K)	0.75320	1.73E-15	0.25500	2.20E-16	0.14270	6.56E-14	1	
pol$^+$ UV	6.80E-13	0.40490	2.55E-06	0.04793	5.81E-10	0.58360	6.98E-13	1

References

[1] M. F. Goodman and B. Tippin, *The expanding polymerase universe.* Nat. Rev. Mol. Cell Biol. **1**, 101 (2000).

[2] F. J. López De Saro, R. E. Georgescu, M. F. Goodman, and M. O'Donnell, *Competitive processivity-clamp usage by DNA polymerases during DNA replication and repair,* EMBO J. **22**, 6408 (2003).

[3] G. Wijffels, B. Dalrymple, K. Kongsuwan, and N. E. Dixon, *Conservation of eubacterial replicases.* IUBMB Life **57**, 413 (2005).

[4] A. Robinson, R. J. Causer, and N. E. Dixon, *Architecture and Conservation of the Bacterial DNA Replication Machinery, an Underexploited Drug Target,* Curr. Drug Targets **13**, 352 (2012).

[5] M. O'Donnell, L. Langston, and B. Stillman, *Principles and concepts of DNA replication in bacteria, archaea, and eukarya.* Cold Spring Harb. Perspect. Biol. **5** (2013), 10.1101/cshperspect.a010108.

[6] V. Pagès and R. P. Fuchs, *How DNA lesions are turned into mutations within cells?* Oncogene **21**, 8957 (2002).

[7] M. D. Sutton, J. M. Duzen, and S. K. Scouten Ponticelli, *A single hydrophobic cleft in the Escherichia coli processivity clamp is sufficient to support cell viability and DNA damage-induced mutagenesis in vivo.* BMC Mol. Biol. **11**, 102 (2010).

[8] A. Vaisman, J. P. McDonald, and R. Woodgate, *Translesion DNA synthesis.* EcoSal Plus **2012** (2012), 10.1128/ecosalplus.7.2.2.

[9] A. Kornberg and T. A. Baker, *DNA Replication* (W. H. Freeman & Co., New York, 1992).

[10] H. Maki and A. Kornberg, *The polymerase subunit of DNA polymerase III of Escherichia coli. II. Purification of the alpha subunit, devoid of nuclease activities.* J. Biol. Chem. **260**, 12987 (1985).

[11] S. Jergic, N. P. Horan, M. M. Elshenawy, C. E. Mason, T. Urathamakul, K. Ozawa, A. Robinson, J. M. H. Goudsmits, Y. Wang, X. Pan, J. L. Beck, A. M. van Oijen, T. Huber, S. M. Hamdan, and N. E. Dixon, *A direct proofreader-clamp interaction stabilizes the Pol III replicase in the polymerization mode.* EMBO J. **32**, 1322 (2013).

[12] J. Courcelle, A. Khodursky, B. Peter, P. O. Brown, and P. C. Hanawalt, *Comparative gene expression profiles following UV exposure in wild-type and SOS-deficient Escherichia coli,* Genetics **158**, 41 (2001).

[13] K. Schlacher and M. F. Goodman, *Lessons from 50 years of SOS DNA-damage-induced mutagenesis.* Nat. Rev. Mol. Cell Biol. **8**, 587 (2007).

[14] Z. Qiu and M. F. Goodman, *The Escherichia coli polB Locus Is Identical to dinA, the Structural Gene for DNA Polymerase II: CHARACTERIZATION OF Pol II PURIFIED FROM A polB MUTANT,* J. Biol. Chem. **272**, 8611 (1997).

[15] K. S.R., M. K., Y. M., G. P., and N. T., *Roles of chromosomal and episomal dinB genes encoding DNA pol IV in targeted and untargeted mutagenesis in Escherichia coli,* Mol. Genet. Genomics **266**, 207 (2001).

[16] R. Woodgate and D. G. Ennis, *Levels of chromosomally encoded Umu proteins and requirements for in vivo UmuD cleavage,* Mol Gen Genet **229**, 10 (1991).

[17] S. Sommer, F. Boudsocq, R. Devoret, and A. Bailone, *Specific RecA amino acid changes affect RecA-UmuD'C interaction,* Mol Microbiol **28**, 281 (1998).

[18] A. Robinson, J. P. McDonald, V. E. A. Caldas, M. Patel, E. A. Wood, C. M. Punter, H. Ghodke, M. M. Cox, R. Woodgate, M. F. Goodman, and A. M. van Oijen, *Regulation of Mutagenic DNA Polymerase V Activation in Space and Time,* PLOS Genet. **11**, e1005482 (2015).

[19] M. D. Sutton, *Coordinating DNA polymerase traffic during high and low fidelity synthesis,* Biochim. Biophys. Acta - Proteins Proteomics **1804**, 1167 (2010).

[20] C. Indiani, M. Patel, M. F. Goodman, and M. E. O'Donnell, *RecA acts as a switch to regulate polymerase occupancy in a moving replication fork,* Proc Natl Acad Sci U S A **110**, 5410 (2013).

[21] A. Furukohri, M. F. Goodman, and H. Maki, *A Dynamic Polymerase Exchange with Escherichia coli DNA Polymerase IV Replacing DNA Polymerase III on the Sliding Clamp,* J. Biol. Chem. **283**, 11260 (2008).

[22] P. J. Hastings, M. N. Hersh, P. C. Thornton, N. C. Fonville, A. Slack, R. L. Frisch, M. P. Ray, R. S. Harris, S. M. Leal, and S. M. Rosenberg, *Competition of Escherichia coli DNA Polymerases I, II and III with DNA Pol IV in Stressed Cells,* PLoS One **5** (2010), 10.1371/journal.pone.0010862.

[23] J. M. Heltzel, R. W. Maul, D. W. Wolff, and M. D. Sutton, *Escherichia coli DNA polymerase IV (Pol IV), but not Pol II, dynamically switches with a stalled Pol III* replicase,* J Bacteriol **194**, 3589 (2012).

[24] M. Patel, Q. Jiang, R. Woodgate, M. M. Cox, and M. F. Goodman, *A new model for SOS-induced mutagenesis: how RecA protein activates DNA polymerase V,* Crit Rev Biochem Mol Biol **45**, 171 (2010).

[25] P. N. Hedde, J. Fuchs, F. Oswald, J. Wiedenmann, and G. U. Nienhaus, *On-line image analysis software for photoactivation localization microscopy.* Nat. Methods **6**, 689 (2009).

[26] J. T. Yeeles and K. J. Marians, *The Escherichia coli replisome is inherently DNA damage tolerant,* Science (80-.). **334**, 235 (2011).

[27] K. Schlacher, M. M. Cox, R. Woodgate, and M. F. Goodman, *RecA acts in trans to allow replication of damaged DNA by DNA polymerase V,* Nature **442**, 883 (2006).

[28] E. M. Witkin, J. O. McCall, M. R. Volkert, and I. E. Wermundsen, *Constitutive expression of SOS functions and modulation of mutagenesis resulting from resolution of genetic instability at or near the recA locus of Escherichia coli,* Mol Gen Genet **185**, 43 (1982).

[29] F. R. Blattner, r. Plunkett G., C. A. Bloch, N. T. Perna, V. Burland, M. Riley, J. Collado-Vides, J. D. Glasner, C. K. Rode, G. F. Mayhew, J. Gregor, N. W. Davis, H. A. Kirkpatrick, M. A. Goeden, D. J. Rose, B. Mau, and Y. Shao, *The complete genome sequence of Escherichia coli K-12,* Science (80-.). **277**, 1453 (1997).

[30] L. C. Huang, E. A. Wood, and M. M. Cox, *Convenient and reversible site-specific targeting of exogenous DNA into a bacterial chromosome by use of the FLP recombinase: the FLIRT system,* J Bacteriol **179**, 6076 (1997).

[31] K. A. Datsenko and B. L. Wanner, *One-step inactivation of chromosomal genes in Escherichia coli K-12 using PCR products.* Proc. Natl. Acad. Sci. U. S. A. **97**, 6640 (2000).

[32] S. H. Chen, R. T. Byrne, E. A. Wood, and M. M. Cox, *Escherichia coli radD (yejH) gene: a novel function involved in radiation resistance and double-strand break repair.* Mol. Microbiol. **95**, 754 (2015).

[33] J. H. Miller, *Experiments in molecular genetics* (Cold Spring Harbor Laboratory Press, 1972).

[34] C. A. Schneider, W. S. Rasband, and K. W. Eliceiri, *NIH Image to ImageJ: 25 years of image analysis,* Nat Methods **9**, 671 (2012).

[35] V. E. a. Caldas, C. M. Punter, H. Ghodke, A. Robinson, and A. M. van Oijen, *iSBatch: a batch-processing platform for data analysis and exploration of live-cell single-molecule microscopy images and other hierarchical datasets,* Mol. BioSyst. (2015), 10.1039/C5MB00321K.

[36] O. Sliusarenko, J. Heinritz, T. Emonet, and C. Jacobs-Wagner, *High-throughput, subpixel precision analysis of bacterial morphogenesis and intracellular spatio-temporal dynamics,* Mol. Microbiol. **80**, 612 (2011).

[37] N. A. Tanner and A. M. van Oijen, *Visualizing DNA replication at the single-molecule level,* Methods Enzym. **475**, 259 (2010).

[38] RCoreTeam, *R: A language and environment for statistical computing*, Tech. Rep. (The R Fondation, Vienna, 2013).